ASIAN JOURNAL OF CIVIL ENGINEERING (BHRC) VOL. 16, NO. 1 (2015)
PAGES 47-66

RELIABILITY EVALUATION OF RC FRAME BY TWO MAJOR FRAGILITY ANALYSIS METHODS

D.C. Haran Pragalath*, R. Davis and P. Sarkar
Department of Civil Engineering, National Institute of Technology Rourkela, Rourkela – 769 008, India

Received: 30 February 2014; **Accepted:** 20 August 2014

ABSTRACT

In the present study two popular approaches for the seismic fragility evaluation of RC buildings are considered. First approach is based on series of time history analysis and a power law representing probabilistic seismic demand model. Second approach is based on Incremental Dynamics Analysis to determine the median collapse intensity measure. The two methods are formulated with different assumptions and methodologies for evaluations. The fragility curves and reliability indices are developed for a typical four storeyed frame by both the approaches and a comparison study is performed. The both methods yield almost the same results at same total dispersions.

Keywords: Fragility; reliability index; peak ground acceleration; performance levels; hazard curve.

1. INTRODUCTION

In the present scenario, structural design codes are shifting towards performance-based methods from the current deterministic approaches. The seismic performance of the designed buildings is significantly influenced by the uncertainties. The uncertainties involved in the design parameters are due to material properties, design intensity of earthquake, loading profiles, quality of construction, modelling uncertainty etc. For reasonably accurate performance assessments analysis in a probabilistic framework is necessary. Probability of exceedance of a damage state by incorporating the uncertainties is studied through a fragility analysis. For conducting a fragility analysis there are different approaches. In the present study two major approaches are selected for the fragility analysis.

(i) In the first approach, the fragility curve is represented by a log normal distribution considering a power law between the intensity measure and the engineering demand parameter

*E-mail address of the corresponding author: haran5441@gmail.com (D.C. Haran Pragalath)

as suggested by [4]. A series of time history analysis is to be performed to estimate the engineering damage parameter as a function of intensity measure.

(ii) In the second approach suggested by [8], the fragility curve is defined by a log normal distribution, with unity median and uncertainty parameter β as the standard deviation, multiplied by the median collapse intensity measure. The median collapse intensity measure is found by conducting series of Incremental dynamic analyses (*IDA*).

In most of Earthquake engineering applications, intensity measure (*IM*) is chosen as Peak Ground Acceleration (*PGA*) or Spectral Acceleration corresponding to first natural period $S_a[T1]$. The fragility curve for the building is combined with the seismic hazard curve for a selected location to find the corresponding reliability index. Seismic hazard curve in Indian subcontinent is partially available. The available hazard curves are in terms of PGA versus annual frequency of exceedance. Hazard curve for a location in the Sikkim-Himalaya, Darjeeling, which is one of the vulnerable regions in India, is selected for the present study.

2. METHODOLOGY

2.1 Assessment of Seismic Reliability

A methodology for the assessment of seismic risk of building structures is presented in [6]. This assessment involves three parts. First part is the identification of the seismic hazard, P [A = a], described by the annual probabilities of specific levels of earthquake motion. Second part is the analysis of global response of the structural system. The response analysis of the structure is carried out by conducting a nonlinear time history analysis for different earthquakes, and the response is expressed in terms of maximum inter-storey drift at any storey. Third part is the calculation of limit state probabilities of attaining a series of (increasingly severe) limit states, LS_i, through the expression:

$$P[LS_i] = \sum_a P[LS_i \mid A = a] P[A = a] \tag{1}$$

The conditional probability $P[LS_i \mid A = a]$ is denoted as the seismic fragility, $F_R(x)$. This conditional probability, explicitly stated, is the probability of meeting or exceeding a specified level of damage, *LS*, given a ground motion which has a certain level of intensity, *a*. This conditional probability is often assumed to follow a two parameter lognormal probability distribution ([4] and [26]).

A point that estimate of the limit state probability for state *i* can be obtained by convolving the fragility $F_R(x)$ with the derivative of the seismic hazard curve, $G_A(x)$, thus removing the conditioning on acceleration as per Eq. 1.

$$P[LS_i] = \int F_R(x) \frac{dG_A}{dx} dx \tag{2}$$

The parameters at the fragility-hazard interface must be dimensionally consistent for the probability estimate to be meaningful. The reliability index for corresponding probability of failure can be found by the following standard Equation as shown below.

$$\beta_{Pf} = -\phi^{-1}\left(P_f\right) \tag{3}$$

$\phi^{-1}(\ )$ is the inverse standard normal distribution.

2.2 Seismic Hazard Analysis

The seismic hazard (G_A) at a building site is displayed through a complimentary cumulative distribution function (*CCDF*). The hazard function is the annual frequency of motion intensity at or above a given level, *x*, to the intensity. Elementary seismic hazard analysis shows that at moderate to large values of ground acceleration, there is a logarithmic linear relation between annual maximum earthquake ground or spectral acceleration, and the probability, $G_A(a)$, that specifies values of acceleration are exceeded. This relationship implies that A is described by following equation suggested by [6],

$$G_A(x) = 1 - \exp[-(x/u)^{-k}] \tag{4}$$

u and *k* are parameters of the distribution. Parameter *k* defines the slope of the hazard curve which, in turn, is related to the coefficient of variation (COV) in annual maximum peak acceleration.

Hazard curve of Darjeeling region, which is one of the most vulnerable earthquake prone areas in India, is developed by [21]. Annual frequency of being exceedance of PGA for Darjeeling Region is shown in Fig. 1. For PGA corresponds to 2500 year return period (2% exceedance probability in 50 years) is found to be 1.58g (marked in Fig. 1).

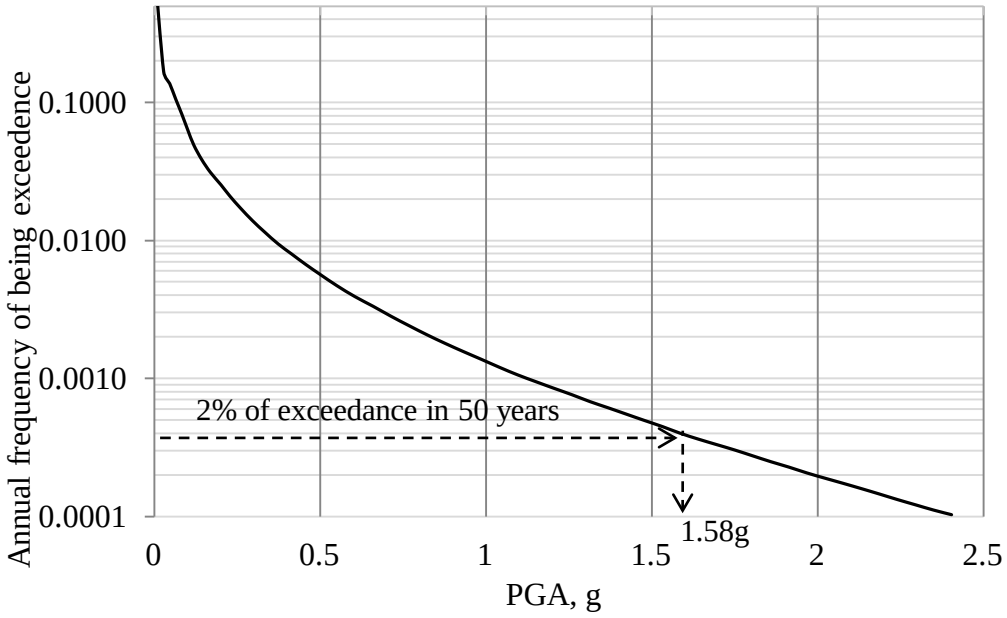

Figure 1. Seismic Hazard curves at the Darjeeling region, India [21].

2.3 Methodologies for Development of Fragility Curves

The fragility function represents the probability of exceedance of a selected Engineering Demand Parameter (*EDP*) for a selected structural limit state (*LS*) subjected to a ground motion intensity measure (*IM*). Fragility curves are cumulative probability distributions that indicate the probability that a component/system will be damaged to a given damage state or a more severe one, as a function of a particular demand. A fragility curve can be obtained for each damage state.

2.3.1 Method I

The seismic fragility, $F_R(x)$ can be expressed in closed form using Eq. 5,

$$P(D \geq C \mid IM) = \phi\left(\frac{\ln \frac{S_D}{S_C}}{\sqrt{\beta_{D|IM}^2 + \beta_c^2}}\right) \tag{5}$$

where, C is the drift capacity, D is the drift demand, S_D is the median of the demand and S_C is the median of the chosen limit state (*LS*). $\beta_{d/IM}$ and β_c are dispersions in the intensity measure and capacities respectively.

Probabilistic Seismic Demand Model (PSDM)

The seismic demand is usually described through probabilistic seismic demand models (*PSDMs*) particularly for nonlinear time history analyses which are given in terms of an appropriate intensity measure (*IM*). In addition to the lognormal assumption, it has been suggested by [4] that the estimate of the median demand, S_D (*EDP*) can be represented in a generalised form by a power model as given in Eq. 6.

$$EDP = a(IM)^b \tag{6}$$

Where, a and b are the regression coefficients of the probabilistic Seismic Demand Model (PSDM). Eq. 5 can be rewritten as Eq. 7 for system fragilities [22] as,

$$P(D \geq C \mid IM) = \phi\left(\frac{\ln IM - \ln IM_m}{\beta_{comp}}\right) \tag{7}$$

where, $IM_m = \exp\left(\frac{\ln S_C - \ln a}{b}\right)$, and the dispersion component, β_{comp} is given as

$$\beta_{comp} = \frac{\sqrt{\beta_{D|IM}^2 + \beta_c^2}}{b} \tag{8}$$

The dispersion $\beta_{D/IM}$ on the data set (d_i) can be calculated using Eq. 9 where $a(IM)^b$ is the best-fit line that represents the mean.

$$\beta_{D|IM} \cong \sqrt{\frac{\sum(\ln(d_i) - \ln(aIM^b))^2}{N-2}} \tag{9}$$

The dispersion in capacity, βc is dependent on the building type and construction quality. [1] suggests values of βc as 0.10, 0.25 and 0.40 depending on the quality of construction good, fair and poor respectively. In this study, dispersion in capacity has been assumed as 0.25, as shown in Table 1.

Limit states define the capacity of the structure to withstand different levels of damage. The median inter-storey drift limit states for RC moment resisting frame structures defining the capacity of the structure at various performance levels (S_C) are suggested by [10]. The median inter-storey drifts for light repairable damage (*IO*), moderate repairable damage (*LS*) and near collapse (*CP*) are listed in Table 1 as suggested by [7], which are considered in the present study.

Table 1: Damage limits and dispersion associated with various structural performance levels [7] and [1]

Limit states designation	Performance levels	Median Inter-storey Drifts S_c for Concrete frames, (%)	Dispersion, β_c
IO	Light repairable damage	1	0.25
LS	Moderate repairable damage	2	0.25
CP	Near collapse	4	0.25

2.3.2 Method II

According to [8], the collapse fragility of each index archetype is defined by the random variable, S_{CT}, assumed to be equal to the product of the median value of the collapse ground motion intensities, $S_{CT}[T]$, as calculated by Incremental nonlinear dynamic analysis [27], and the random lognormal variable, $\lambda_{TOT.}$

$$S_{CT} = S_{CT}[T]\lambda_{TOT} \tag{10}$$

Where, λ_{TOT} is a lognormal random variable with median value of unity and a lognormal standard deviation of β_{TOT}. The lognormal random variable is assumed to be the product of four component random variables:

$$\lambda_{TOT} = \lambda_{RTR}\lambda_{DR}\lambda_{TD}\lambda_{MDL} \tag{11}$$

where, $\lambda_{RTR,}$ λ_{DR}, λ_{TD} and $\lambda_{MDL,}$ are lognormal random variables with median values of unity, and lognormal standard deviation parameters, β_{RTR} , β_{DR} , β_{TD} and β_{MDL} respectively. Since these parameters are assumed to be statistically independent, the lognormal standard deviation parameter, β_{TOT}, describing total collapse uncertainty, is given by:

$$\beta_{TOT} = \sqrt{(\beta_{RTR})^2 + (\beta_{DR})^2 + (\beta_{TD})^2 + (\beta_{MDL})^2} \tag{12}$$

where,
β_{TOT}= total system collapse uncertainty (0.20- 0.95)
β_{RTR}= record-to-record collapse uncertainty (0.20- 0.40)
β_{DR}= design requirements related collapse uncertainty (0.10- 0.50)
β_{TD}= test data related collapse uncertainty (0.10 - 0.50)
β_{MDL}= modelling related to collapse uncertainty (0.10 – 0.50)

This approach is used by many studies for the development of fragility curves at collapse limit state for various archetypical buildings [24]. Though this method is discussed about the fragility curve only at collapse, but in the present study this method is used for fragility curve at various limit states such as IO, LS and CP as mentioned in Method I for comparison purposes.

3. EXAMPLE FRAMES

A brief history of development of Indian Seismic code is presented in [14]. Based upon the intensity of past earthquakes, Indian Seismic code [12] divided the entire country into four zones at present namely, zone II, III, IV and V with PGAs 0.1g, 0.18g, 0.24g and 0.36g respectively. The building frame considered for numerical analysis in the present study is assumed to be located in the most severe seismic zone of India, zone V (with medium soil conditions). The design peak ground acceleration (PGA) of this zone is specified as 0.36*g*. Seismic loads are estimated as per [12] and the design of the RC elements are carried out as per [13]. The characteristic strength of concrete and steel are taken as 25MPa and 415MPa. The buildings are assumed to be symmetric in plan, and hence a single plane frame is considered to be representative of the building along one direction. Typical bay width and column height in this study are selected as 5m and 3.2m respectively, as observed from the study of typical existing residential buildings. A configuration of 4 stories and 4 bays (4s4b) is considered. Fig. 2 shows the building frame configuration and details of beams and columns. The dead load of the slab (5 m × 5 m panel) including floor finishes is taken as 3.75 kN/m^2 and live load as 3 kN/m^2. The design base shear (V_B) is calculated as follows [12].

$$V_B = \left(\frac{Z}{2} \frac{I}{R} \frac{s_a}{g} \right) W \tag{13}$$

Where, seismic zone factor, Z = 0.36, Importance factor I = 1.0, Response reduction factor R = 5.0. W = Seismic weight of building and S_a/g = Spectral acceleration from the design response spectrum corresponding to fundamental natural period of the building normalised to acceleration due to gravity.

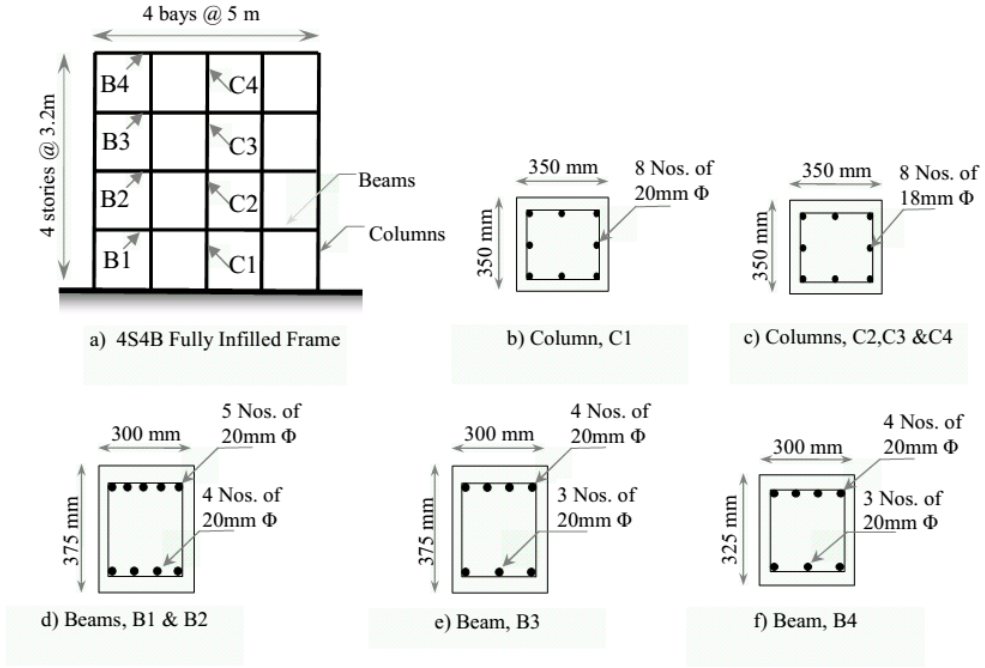

Figure 2. Typical 4S4B-Infilled frame and its corresponding reinforcement details

4. MODELLING FOR NONLINEAR ANALYSIS

As per the methodology adopted a series of Nonlinear Dynamic Time History Analysis of the example frame is required. Opensees Laboratory tool developed by [26] and available at NEEShub is used for the present study. In order to validate the modelling and analysis approach, a validation study is conducted.

4.1 Validation study

A full-scale reinforced concrete bridge column reported in [2] was chosen for validation study. The selected Bridge Model as shown in Fig. 4a was tested on the NEES Large High Performance Outdoor Shake Table at UCSD's Englekirk Structural Engineering Center under dynamic conditions, (http://nisee2.berkeley.edu/peer/prediction_contest/) as part of a blind prediction contest. Six unidirectional earthquake ground motions, starting with low intensity shaking, were increased so as to bring the pier progressively to near collapse conditions. Detailed information about geometry and material properties may be found in [2] and [25].

Force-based nonlinear beam-column elements that consider the spread of plasticity along the element were used to model the columns and Beams. Formulation of the fiber-based element is explained in [16] and [15] has studied sensitivity study about the number of integration points in each element and suggest to used five integration points. In the present study number of integration points considered for each element is chosen as five. Fig. 3a shows the element discretisation and Fig. 3b shows the section discretisation of fiber based modelling for Reinforced concrete.

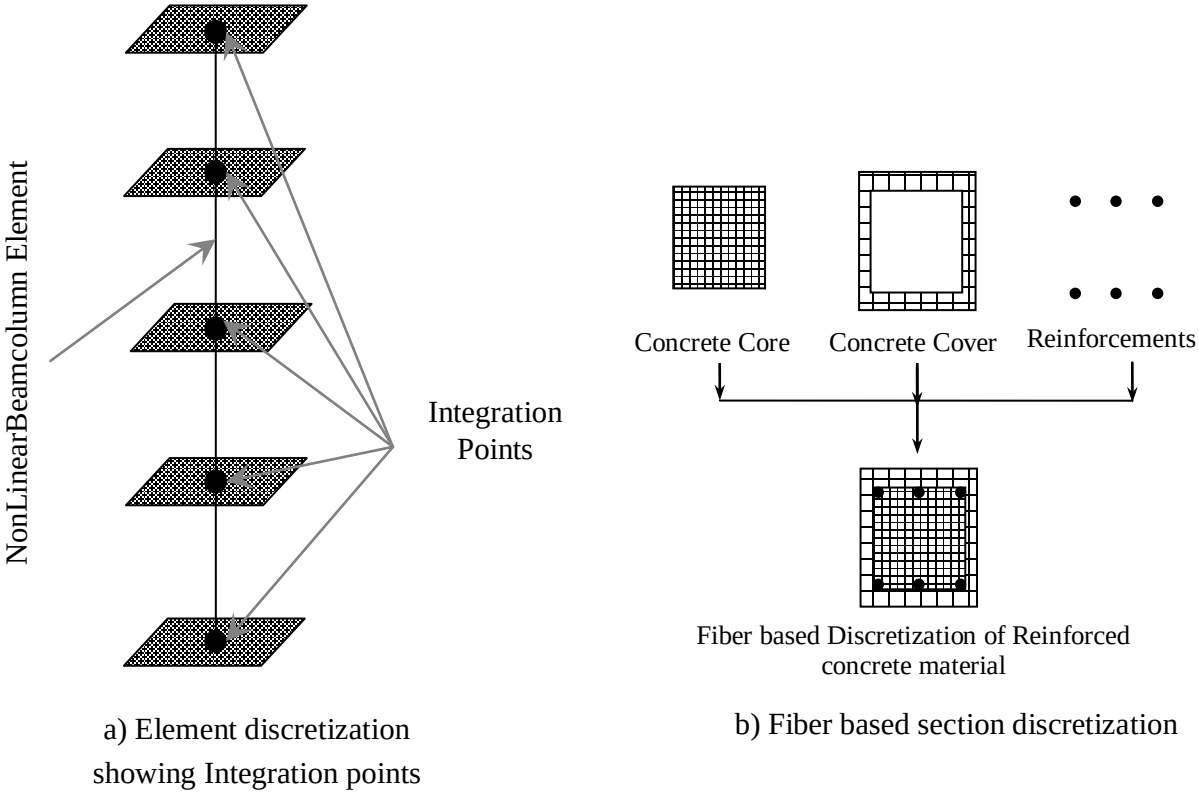

Figure 3. Computational model, Element, Sectional discretization of force-based nonlinear beam-columns utilized to model Building columns and beams

Opensees Library have various in-built uniaxial stress-strain curves for different materials. Concrete is modelled using concrete01 (Kent-Scott-Park concrete material object with degraded linear unloading/reloading stiffness and no tensile strength) material model where the parameters required to define model are maximum stress (f_{cc}) and corresponding to strain (ε_{cc}), ultimate strain (ε_{cu}) and corresponding stress (f_{cu}). The initial slope (E_i) of the curve is taken as two times of the secant modulus. The secant modulus is calculated as ratio of maximum stress to strain corresponding to maximum stress ($E_i = 2.f_{cc}/\varepsilon_{cc}$). The strength degradation is assumed to be linear function of unloading/reloading stiffness. Reinforcement is modelled using steel02 material which is a uniaxial Giuffre-Menegotto-Pinto steel material object with isotropic strain hardening. 1% of tangent stiffness proportional damping is applied as global damping for the first mode shape as reported in [25]. Fig. 4b shows the computational model developed in Opensees platform. In this validation study, only one unidirectional earthquake time history shown in Fig. 5a is chosen. Fig. 5b shows displacement histories obtained form both experimental and computational study. It can be seen that the computational displacement history is fairly matching with the experimental results though there is some difference in the post-peak region.

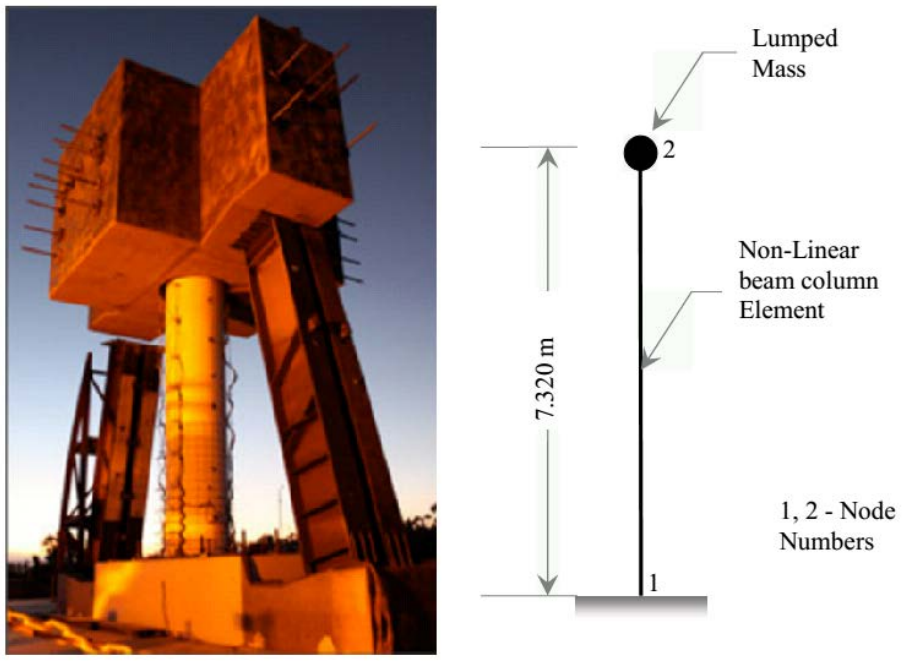

a) Model tested on the NEES Large High Performance Outdoor Shake Table at UCSD's Englekirk Structural Engineering Center (http://nisee2.berkeley.edu/peer/prediction_contest/)

b) Computation Model in Opensees Platform

Figure 4. Experimental model and Computation model of Reinforced concrete bridge column

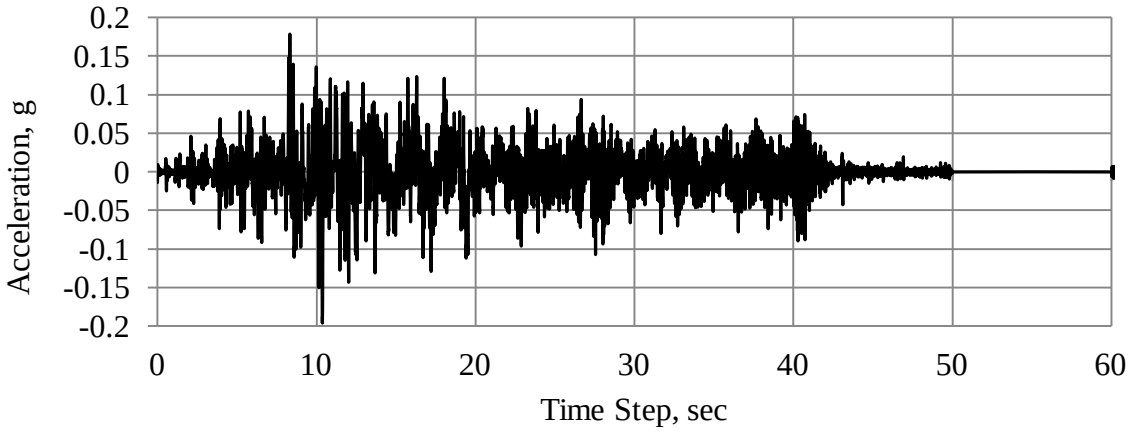

a) Earthquake ground motion [25]

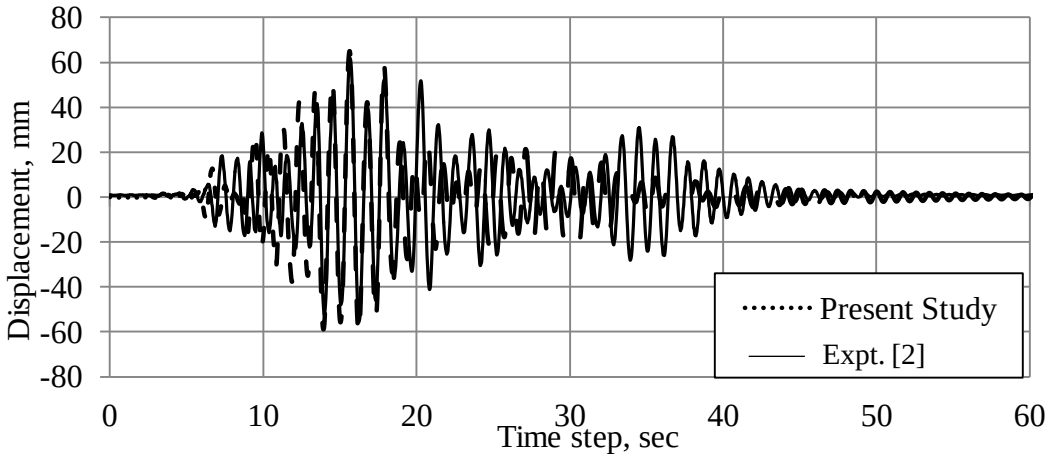

b) Experimental and computational responses of RC Bridge column

Figure 5. Time History Data and corresponding Displacement History

4.2 Structural Modelling, Earthquake Data and Material Uncertainty

A computational model of the selected frame (4s4b) is developed as per the validated modelling approach. Selection of Earthquake for a Dynamic analysis is more challenging task as each earthquake has its unique property as it involves so many uncertainties. [11] has worked on selection of earthquakes for time history analysis and shared time history data for far field and near field ground motions. Structural collapse typically occurs at extremely large levels of ground motion, so this ground motion set was selected to represent these extreme motions to the extent possible. More about the selection of earthquake can be found in [8]. Regarding number of earthquakes required for developing fragility curves, there are no clear guidelines reported in the literature. [1] recommends a suite of 11 pairs of ground motions for a reliable estimate of the response quantities. [4] suggests 30 recorded ground motions to meet the spectral matching criteria for Nuclear Power Plant infrastructures. [14] used 40 ground motions for developing fragility curves. In the present study, twenty two pair (44 ground motions) of Far-Field natural Ground Motions collected from [11] are used for the Nonlinear dynamic analysis for both the methods.

These Earthquakes are converted to match with Indian Spectrum [12] using a program, WavGen developed by [20]. WavGen uses a wavelet-based procedure to decompose a recorded accelerogram into a desired number of time-histories (response spectrum compatible) with non-overlapping frequency contents such that the temporal variations in its frequency content are retained in the synthesized accelerogram. Fig. 6 shows the response spectrums for 44 converted ground motions along with Indian spectrum.

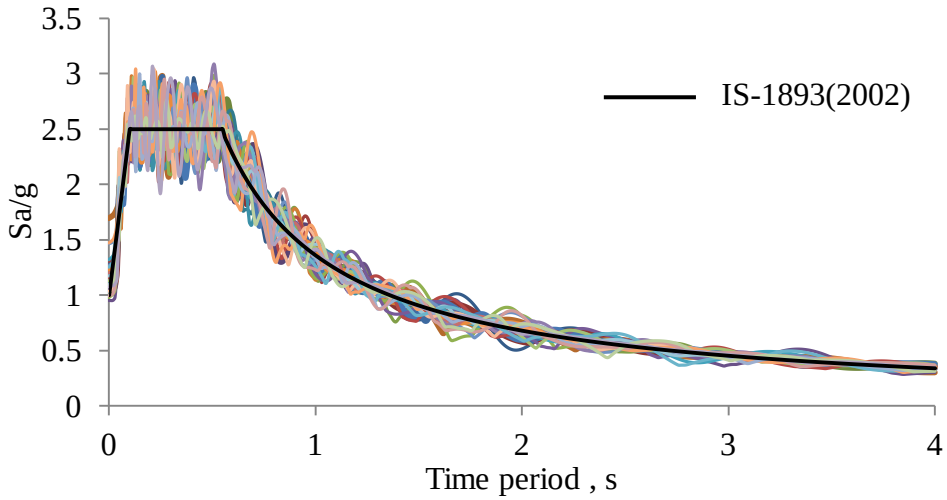

Figure 6. Response Spectra for 44 converted ground motions along with Indian code[12] design spectrum

Material properties of concrete, and steel used in the construction and the global structural damping are random in nature. Table 2 shows the mean and co-efficient of variation (COV) for each random variable considered. The statistical parameters for concrete and steel are taken from [23] for Indian conditions. 5% is considered as mean value of global damping (modeled as Rayleigh damping) with COV of 40% as suggested by [5]. A set of 44 values for each random variable are generated using Latin Hypercube Sampling (*LHS*) [17] as 44 models are considered for developing Fragility curves.

Table 2: Details of random variables used in LHS scheme

Material/Property	Variable (MPa)	Mean	COV (%)	Distribution	Remarks
Concrete	f_{ck}	30.28	21.0	Normal	Uncorrelated
Steel	f_y	468.90	10.0	Normal	Uncorrelated
Global Damping	ξ	5%	40.0	Normal	Uncorrelated

5. FRAGILITY CURVES BY TWO APPROACHES

With regard to method I, 44 computational models are generated. The 44 ground motions are scaled linearly from 0.1g to 1.0g and each computational model is analysed for a particular earthquake (randomly selected) with a particular PGA. A total of 44 nonlinear dynamic time history analyses are performed which took approximately 14 hrs of computational time on a standard personal computer. The maximum inter-storey drift (*EDP*) at any storey is monitored and plotted in logarithmic graph along with the corresponding PGA (IM) as shown in Fig. 7a. A power law (refer Eq. 6) relationship is fitted using regression analysis, which represents the *PSDM* model. The regression coefficients *a* and *b* are found to be 167.19 and 1.2114 respectively. The R^2 value for the fitted relation is found to be 0.82. The

dispersion, $\beta_{D/IM}$ is calculated using the Eq. 9 and found to be 0.351. The uncertainty in the capacity and demand are incorporated in the Method I by considering the dispersions $\beta_{D/IM}$ and β_C. The total dispersion (β_{TOT}) for method I, is calculated as $\sqrt{\beta_{D|IM}^2 + \beta_c^2}$ and is found to be 0.431. The fragility curves for each limit states (*IO*, *LS* and *CP*) are developed using the closed form Eq. 7 as shown in Fig. 7b.

For method II, the incremental dynamic analyses of the same 44 computational models are performed using the same 44 ground motions for PGAs of 0.1g to 1.2g with an increment of 0.1g. A total of 528 nonlinear dynamic time history analyses are performed which took approximately 176 hrs of computational time on a standard personal computer. The maximum inter-storey drift at any storey level at each PGAs are recorded and plotted along with corresponding spectral accelerations, S_a at 5% damping at fundamental natural period (*T1*) is shown in Fig.8. The median $S_{CT}(T)$ at each limit state *IO*, *LS* and *CP* are found out as 0.236g, 0.432g and 0.695g respectively. The values of dispersions β_{RTR} , β_{DR} , β_{TD} and β_{MDL} (refer section 3.2) are suggested by [8] for different situations. Accordingly the values of these dispersions are assumed as 0.2 (section 7.3.1 of [8]), 0.25 (Table 3-1 of [8]), 0.35 (Table 3-2 of [8]) and 0.35 (Table 5-3 of [8]) respectively for β_{RTR} , β_{DR} , β_{TD} and β_{MDL} and the corresponding β_{TOT} is found to be 0.589 using Eq. 12. Fragility curves in terms of *Sa[T1]* are developed using the Eq. 10 for various limit states as shown in Fig. 9a. The method II uses the intensity parameter *as Sa[T1]*, while the seismic hazard curves are available in terms of PGA. Due to this reason fragility curves are expressed in terms of PGA as the intensity measure as shown in Fig. 9b.

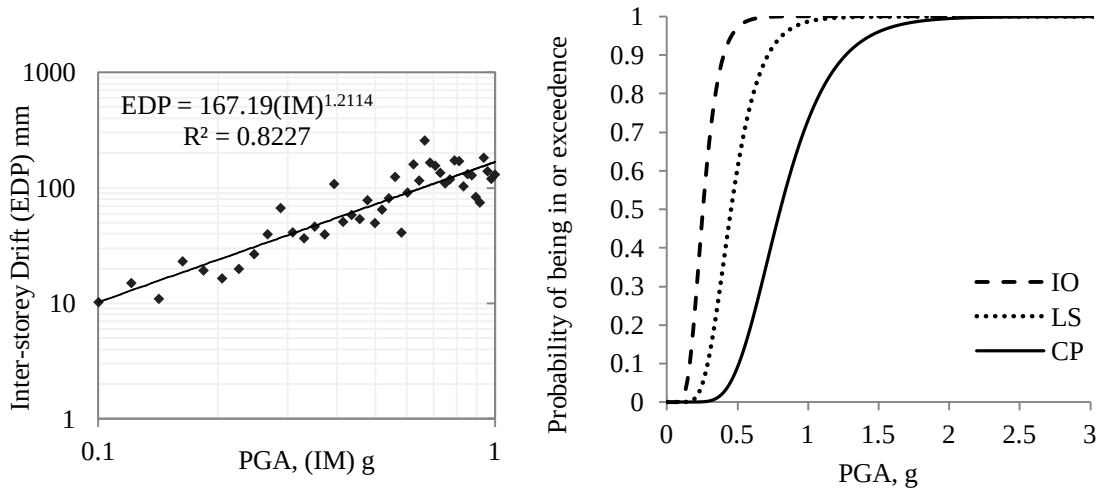

(a) PSDM Model (b) Fragility curve

Figure 7. PSDM Model and Fragility Curve by Method I (β_{TOT} = 0.431)

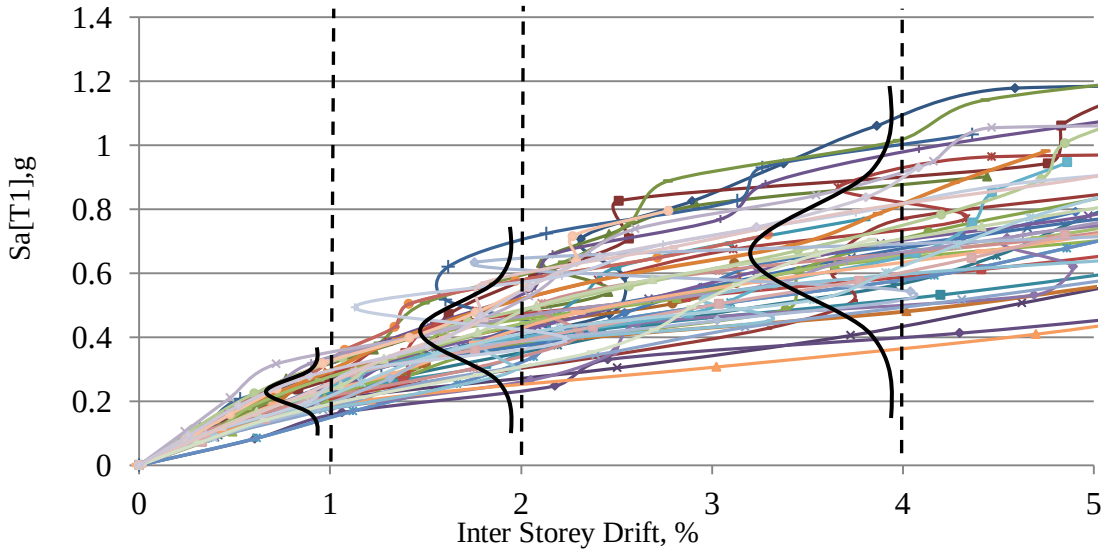

Figure 8. *IDA* curves for the frame considered

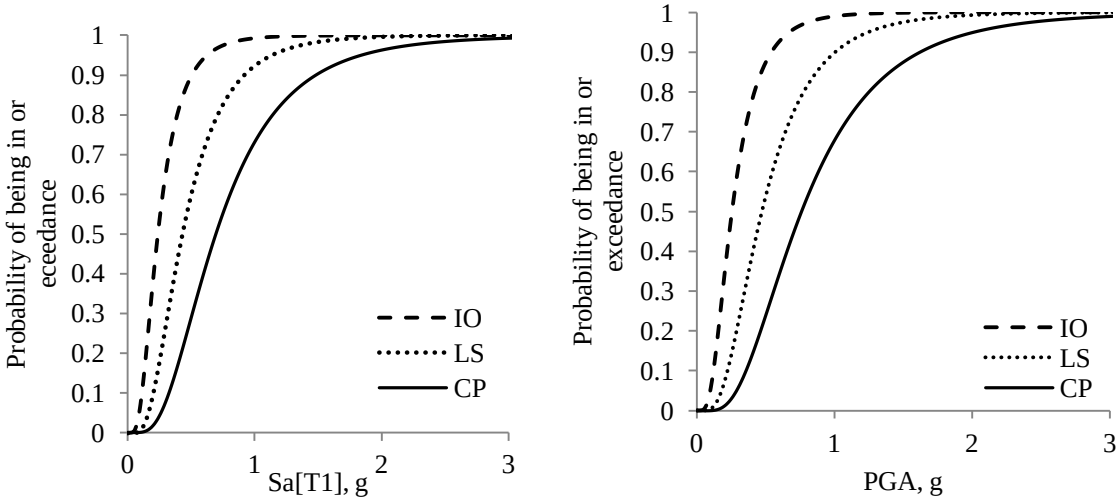

(a) Fragility curve in terms of Sa[T1] (b) Fragility curve in terms of PGA

Figure 9. Fragility Curve by Method II (β_{TOT}=0.589)

6. COMPARISON OF FRAGILITY CURVES BY TWO APPROACHES

Method I and Method II use two different approaches for the development of fragility curves. PGA values corresponding to 50% of probability of exceedance from the fragility curves obtained using two Methods are found to be 0.80g and 0.76g for method I and Method II respectively as marked in Fig. 10.

While Method I uses the assumption of power law and consideration of dispersions using two types of dispersion parameters, the Method II uses the median spectral acceleration at different limit states calculated from IDAs, with four types of dispersions for uncertainty

considerations. In order to see the comparison of fragility curves by both methods, the fragility curves developed at near collapse limit state is drawn in the same plot as shown in the Fig. 10. The corresponding dispersions $\beta_{D/IM}$ and β_C for method I and β_{RTR}, β_{DR}, β_{TD}, and β_{MDL} for Method II are shown. The total dispersion (β_{TOT}) in each method is not the same.

As it is more logical to compare the fragility curves developed by two methods with the same dispersions, the types of dispersions in method II are also reduced to two (β_{MDL} and β_{DR}) similar to the two dispersions ($\beta_{D/IM}$ and β_C) considered in method I. The fragility curves thus developed are shown in Fig. 11 with corresponding values of dispersions. It can be observed that difference in Probability of exceedance for each PGAs for both fragility curves is almost negligible.

In a similar way, the two types of dispersions (β_{RTR}, β_{TD}) are added in method I to make totally four types of dispersions ($\beta_{D/IM}$, β_C, β_{RTR}, β_{TD}) similar to the four dispersions (β_{RTR}, β_{DR}, β_{TD}, and β_{MDL}) considered in method II. The corresponding fragility curves are shown in Fig. 12 along with the dispersion values. In this case also, it can be seen that the difference in Probability of exceedance for each PGAs for both fragility curves is almost negligible.

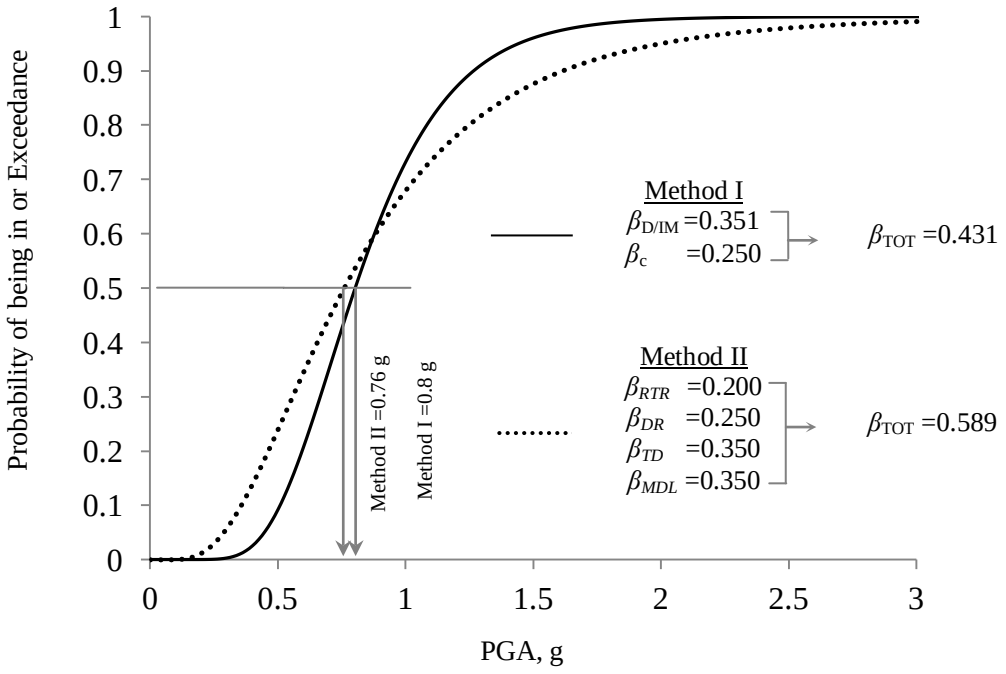

Figure 10. Fragility Curves for CP performance level by Method I (β_{TOT} =0.431) and Method II (β_{TOT} =0.589)

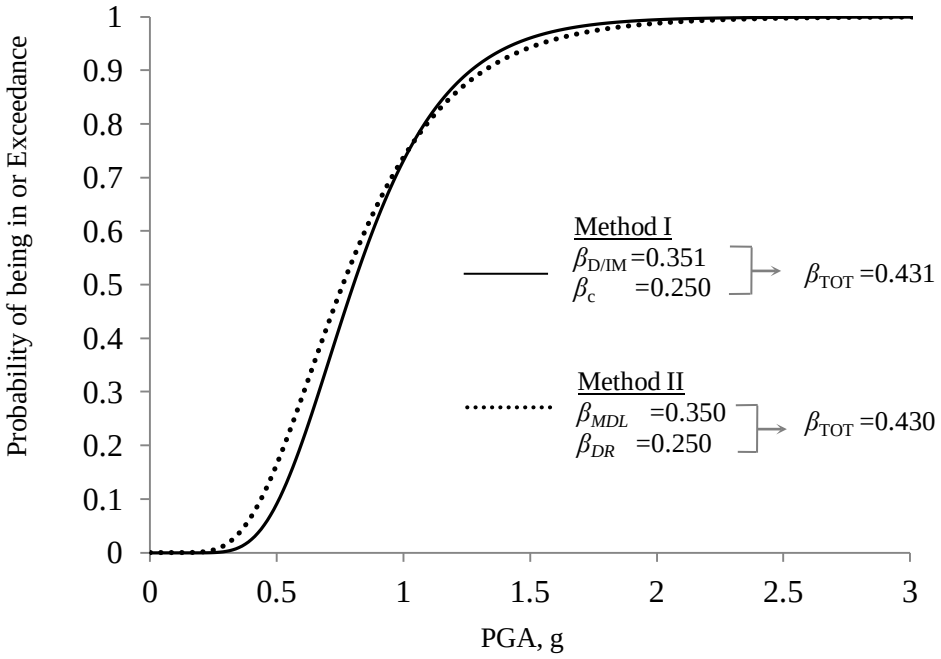

Figure 11. Fragility Curves for CP performance level by Method I (β_{TOT} =0.431) and Method II (β_{TOT} =0.430)

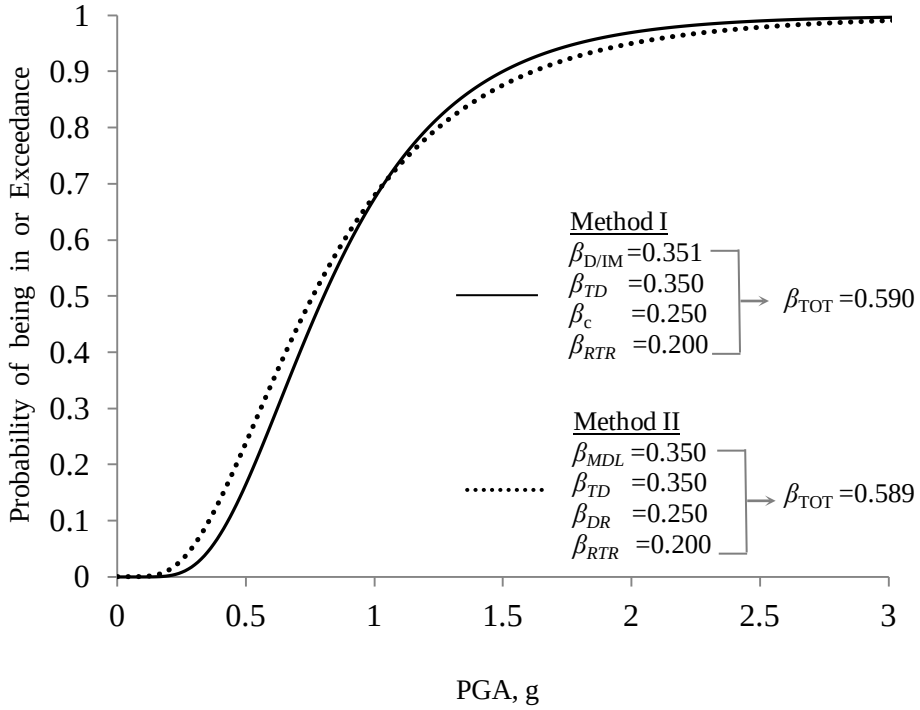

Figure 12. Fragility Curves for CP performance level by Method I (β_{TOT} =0.590) and Method II (β_{TOT} =0.589)

7. RELIABILITY INDEX

In order to understand the effect of dispersion values (considered in the fragility curves by two approaches) quantitatively, the fragility curves are combined with an appropriate hazard curve to form corresponding reliability indices. The Reliability indices are estimated by combining the fragility curve for a particular limit states with hazard curves using the Eq. 2. In present study, Darjeeling seismic Hazard curve is chosen for Reliability Index estimation. PGA corresponds to 2% annual probability of occurrence in 50 years is found to be 1.58g from the hazard curve (Fig. 1).

Reliability Index is calculated for both the methods of fragility curves for collapse prevention level considering two dispersions ($\beta_{D/IM}$ and β_C) in Method I and four dispersions in Method II ($\beta_{D/IM}$, β_C, β_{RTR}, β_{TD}) as shown in Fig.13. The corresponding dispersions $\beta_{D/IM}$ and β_C for method I and β_{RTR}, $\beta_{DR,}$ β_{TD}, and β_{MDL} for Method II are also shown in the Fig. 13. It can be seen that as the PGA increases the reliability index decreases as logically expected. The reliability indices corresponding to a PGA of 1.58g is found to be 2.82 (β_{TOT} = 0.431) and 2.66 (β_{TOT} = 0.589) for method I and Method II respectively (refer Table 3). The reliability index calculated from the fragility curve of Method II is less due to higher value of total dispersion and lower median value of the intensity measure. The percentage difference in reliability index of Method I with reference to that of method II is about 6.01%.

As explained earlier, it will be more logical to compare the reliability indices developed by two methods with the same dispersions, the types of dispersions in method II are reduced to two (β_{MDL} and β_{DR}) similar to the two dispersions ($\beta_{D/IM}$ and β_C) considered in method I. The corresponding reliability indices are shown in Fig. 14 with corresponding values of dispersions. It can be observed that difference in reliability indices at each PGA are less than that of the previous case (Fig. 13). The reliability indices corresponding to a PGA of 1.58g is found to be 2.82 (β_{TOT} = 0.431) and 2.75 (β_{TOT} = 0.430) for method I and Method II respectively (refer Table 3). The percentage difference in reliability index of method I with reference to that of Method II is reduced to about 2.54% when total dispersions are same with two types of dispersion parameters.

Likewise, the two types of dispersions (β_{RTR}, β_{TD}) are added in method I to make totally four types of dispersions ($\beta_{D/IM}$, β_C, β_{RTR}, β_{TD}) similar to the four dispersions (β_{RTR}, $\beta_{DR,}$ β_{TD}, and β_{MDL}) considered in method II. The reliability indices considering four types of dispersions in the two methods are shown in Fig. 15. It can be seen that reliability indices at each PGA are found closer. The reliability indices corresponding to a PGA of 1.58g is found to be 2.75 (β_{TOT} = 0.590) and 2.66 (β_{TOT} = 0.589) for method I and Method II respectively (refer Table 3). The percentage of difference in reliability index of method I with reference to that of Method II is reduced to about 3.38% when total dispersions are same with four types of dispersion parameters.

It can be inferred from the Fig. 14 and 15 that both methods can give identical results when the total dispersions considered in Method I and Method II are almost same. It is observed from Fig. 13 that dispersion plays a major role to obtain more realistic values of reliability index.

Table 3: Dispersions considered in two methods and its corresponding Reliability Index for the level of severe damage

Dispersions	β_{MDL} *(or)* $\beta_{EDP/IM}$	β_{TD}	$\beta_{DR\,(or)}\,\beta_c$	β_{RTR}	β_{TOT}	Reliability Index for 2% Exceedance in 50 years
Method I	$0.351^{*}(\beta_{EDP/IM})$	--	$0.250^{\$}(\beta_c)$	--	0.431	2.82
	$0.351^{*}(\beta_{EDP/IM})$	$0.350^{\#}$	$0.250^{\$}(\beta_c)$	$0.200^{\#}$	0.590	2.75
Method II	$0.350^{\#}(\beta_{MDL})$	--	$0.250^{\#}(\beta_{DR})$	--	0.430	2.75
	$0.350^{\#}(\beta_{MDL})$	$0.350^{\#}$	$0.250^{\#}(\beta_{DR})$	$0.200^{\#}$	0.589	2.66

*calculated, $^{\#}$assumed as per [8], $^{\$}$assumed as per [1]

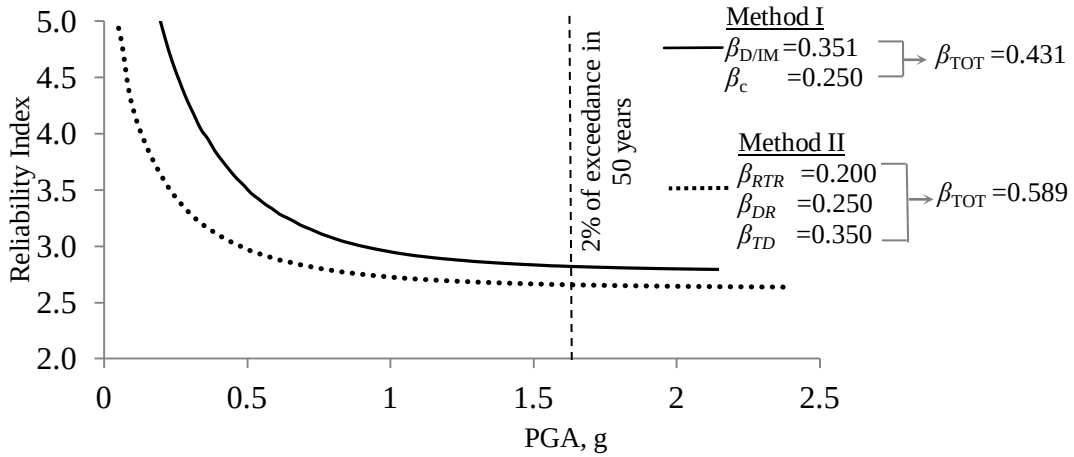

Figure 13. Comparison of Reliability Index for CP performance level by Method I (β_{TOT} =0.431) and Method II (β_{TOT} =0.589)

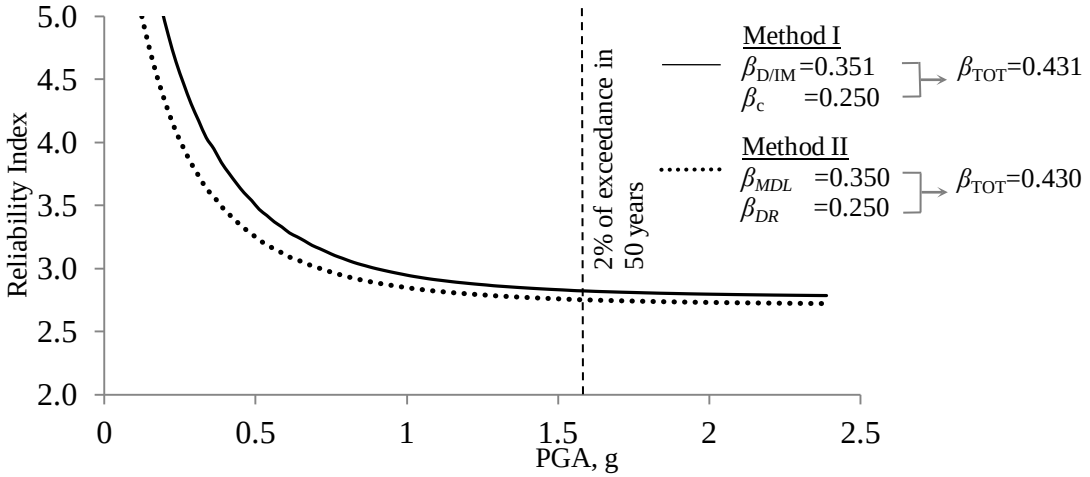

Figure 14. Comparison of Reliability Index for CP performance level by Method I (β_{TOT} =0.431) and Method II (β_{TOT} =0.430)

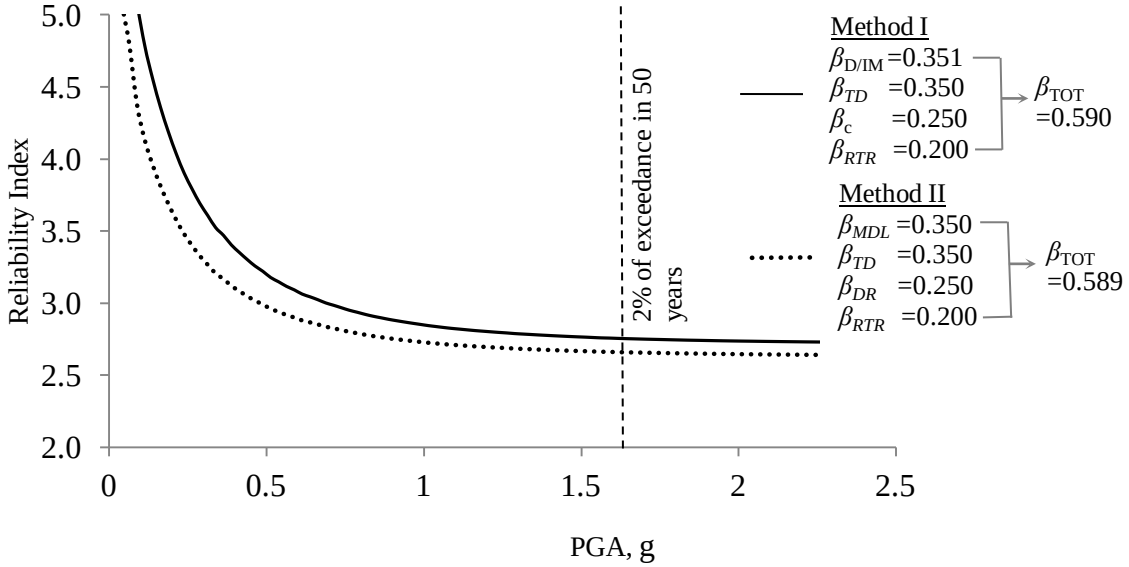

Figure 15. Comparison of Reliability Index for CP performance level by Method I (β_{TOT} =0.590) and Method II (β_{TOT} =0.589)

8. CONCLUSIONS

In the present study two different approaches for the fragility evaluation are selected. First approach is based on series of time history analysis and a power law representing probabilistic seismic demand model. Second approach is based on Incremental Dynamics Analysis to determine the median collapse intensity measure. The total computational time taken for nonlinear dynamic time history analysis for Method I is about 8% that of Method II. From the fragility curves developed by both methods it is observed that PGA values corresponding to 50% of probability of exceedance are found to be almost closer. This implies that the power law assumption [5] used in Method I is more rational.

It is observed that the Method I consider the dispersions with two parameters ($\beta_{D/IM}$ and β_C) and method II consider same with four types ($\beta_{D/IM}$, β_C, β_{RTR}, β_{TD}). It was found that the inherent dispersions considered in the two fragility methods lead to significant changes in the exceedance probabilities given by the two fragility curves. When the same types of dispersions are included in each method, the difference in fragility curves is reduced.

Comparison of the two approaches is studied quantitatively using reliability indices obtained by combining the respective fragility curves with an appropriate hazard curve. When the same types of dispersions are included in each method, the difference in reliability indices curves is reduced to 2.5%-3.4% from a initial value of 6.01%.

Acknowledgements: The Authors acknowledge the support of NEEShub for allowing the access to the OpenSees Laboratory tool [9] and the financial support (Sanction No. SB/FTP/ETA-445/2012) received from SERB, Department of Science and Technology, Government of India.

REFERENCES

1. ATC 58 50% Draft. Guidelines for seismic performance assessment of buildings, *Applied Technology Council*, Redwood City, CA, 2009.
2. Bianchi F, Sousa R, Pinho R. Blind prediction of a full –scale RC bridge column tested under dynamic conditions, *Proceedings of 3rd International Conference on Computational Methods in Structural Dynamics and Earthquake Engineering Corfu*, Greece, 2011, Paper No. 294.
3. Celik OC, Ellingwood BR. Seismic fragilities for non-ductile reinforced concrete frames–Role of aleatoric and epistemic uncertainties, *Structural Safety*, **32**(2010) 1-12.
4. Cornell CA, Jalayer F, Hamburger RO, Foutch DA. The Probabilistic Basis for the 2000 SAC/FEMA Steel Moment Frame Guidelines, *Journal of Structural Engineering*, **128**(2002) 526-33.
5. Davenport AG. Hill-Carroll Damping in tall buildings: its variability and treatment in design, *ASCE Spring Convention*, Seattle, USA, Building Motion in wind, (1986)42-57.
6. Ellingwood BR. Earthquake risk assement of building structures, *Reliability Engineering and System Safety*, **74**(2001) 251-62.
7. FEMA 356. Pre-standard and commentary for the seismic rehabilitation of buildings, *American Society of Civil Engineers*, USA, 2000.
8. FEMA P695. *Quantification of Building Seismic Performance Factors, prepared by the Applied Technology Council*, Redwood City, California for the Federal Emergency Management Agency, Washington, D.C, 2012.
9. Frank M, Christopher M, Pedro A, Joseph AH. Open Sees Laboratory, https://nees.org/resources/openseeslab, 2014.
10. Ghobarah A. Performance-based design in earthquake engineering: state of development, *Engineering Structures*, **23**(2000) 878-84.
11. Haselton CB, Whittaker AS, Hortacsu A, Baker JW, Bray J, Grant DN. Selecting and scaling earthquake ground motions for performing response-history analyses, *Proceedings of the 15th World Conference on Earthquake Engineering*, Lisboa, Portugal, 2012.
12. IS 1893 Part I. Indian standard criteria for earthquake resistant design of structures, *Bureau of Indian Standards*, New Delhi, 2002.
13. IS 456. Indian standard for plain and reinforced concrete code of practice, *Bureau of Indian Standards*, New Delhi, 2000.
14. Jain SK, Nigam NC. Historical developments and current status of earthquake engineering in india, *Proceedings of the 12th World Conference on Earthquake Engineering*, Auckland, New Zealand, 2000.
15. Kunnath SK. Application of the PEER PBEE methodology to the I-880 viaduct, *Pacific Earthquake Engineering Research Center*, College of Engineering, University of California, Berkeley, 2007.
16. Lee TH, Mosalam KM. Probabilistic fiber element modeling of reinforced concrete structures, *Computers and Structures*, **82**(2004) 2285-99.
17. MatLAB. MatLab-Programming software for all kind of problems [online]. < http:// www.mathworks.com/>, 2012.

18. Mander JB, Priestley MJN, Park R. Theoretical stress-strain model for confined concrete, *Journal of Structural Engineering*, **114**(1988) 1804-26.
19. Menegotto M, Pinto PE. Method of analysis for cyclically loaded R.C. plane frames including changes in geometry and non-elastic behaviour of elements under combined normal force and bending, *Symposium on the Resistance and Ultimate Deformability of Structures Acted on by Well Defined Repeated Loads*, International Association for Bridge and Structural Engineering, Zurich, Switzerland, (1973) 15-22.
20. Mukherjee S, Gupta VK. Wavelet-based generation of spectrum compatible time histories, *Soil Dynamics and Earthquake Engineering*, **22**(2002) 799-804.
21. Nath SK, Adhikari MD, Maiti SK, Devaraj N. Seismic hazard and risk microzonation of darjeeling-sikkim himalaya, *Natural Hazards*, 2013, Under review.
22. Nielson BG. *Analytical Fragility Curves for Highway Bridges in Moderate Seismic zones*, Ph.D. Thesis, Georgia Institute of Technology, 2005.
23. Ranganathan R. Structural Reliability Analysis and Design, Jaico Publishing House, Mumbai, 1999.
24. Ravichandran SS. *Design provisions for Autoclaved aerated Concrete Infilled Steel Moment frames*, PhD Dissertation, University of Texas, Austin, 2009.
25. Seismosoft. SeismoStruct v6.0 - Verification Report. Available from URL: www.seismosoft.com, 2013.
26. Song J, Ellingwood BR. Seismic reliability of special moment steel frames with welded connections: II, *Journal of Structural Engineering*, **125**(1999) 357–71.